

Chapter 2

Surface Acoustic Wave Motor Modeling and Motion Control

Minoru Kuribayashi KUROSAWA¹

Abstract For miniaturization of ultrasonic transducers, a surface acoustic wave device has an advantage in rigid mounting and high-power-density operation. A surface acoustic wave (SAW) motor has been investigated, and its superior performances have been demonstrated. From investigations based on experiments, it was found that slider surface texture affects motor performances such as speed and thrust. Theoretically, however, the effect of the physical property of a slider-textured surface on motor performance had not been investigated sufficiently. A physical modeling of the SAW motor has been attempted, one slider projection was modeled including the compliance of the slider and stator materials, and also the stick and slip at the boundary. Using the slider projection modeling, operations of the SAW motor were simulated, and then, the results were compared with the experimental results. For servo control system application, a feed back controller compensating a nonlinear dead zone of the motor is reported. The feed back controller is simple and very effective. For an advanced motion control, a precise modeling of the SAW motor has been studied.

2.1 Introduction

For miniaturization of ultrasonic transducers, a surface acoustic wave device has an advantage in rigid mounting and high-power-density operation. A surface acoustic wave (SAW) motor has been investigated [1-4], and its superior performances have been demonstrated: a speed of 1.5 m/s [5], a thrust of 12 N [4], and a stepping motion of 0.5 nm [6, 7] in the case of using a 60x14x1 mm³ plate piezo-electric transducer. In addition, to increase the application range, a higher operation frequency of 100 MHz [8] and a two-dimensional design [9] were investi-

¹ Minoru Kuribayashi KUROSAWA

Interdisciplinary Graduate School of Science and Engineering, Tokyo Institute of Technology

gated. In addition, to reduce power consumption, energy circulation driving has been proposed [10] and investigated [11].

From investigations based on experiments, it was found that slider surface texture affects motor performances such as speed and thrust [3-5]. Theoretically, however, the effect of the physical property of a slider-textured surface on motor performance had not been investigated sufficiently [12].

Physical modeling of the SAW motor has been attempted, one slider projection was modeled including the compliance of the slider and stator materials [13], and also the stick and slip at the boundary. Using the slider projection modeling, operations of the SAW motor were simulated, and then, the results were compared with the experimental results.

For servo control system application, not only for the efficiency improvement from electric power to mechanical output, an energy circulation driving is important [14]. Traveling wave excitation and the motor operation has been reported already. In the following section, feed back controller compensating a nonlinear dead zone of the motor is reported [15, 16]. The feed back controller is simple and very effective. For an advanced motion control, a precise modeling of the SAW motor has been studied.

2.2 Principle

If we use a Rayleigh wave for a surface acoustic wave actuator, a basic device construction for the motor is shown in Fig.2.1. The actuator has only a thin plate transducer and a thin friction material. The plate transducer is a surface acoustic wave device to generate a Rayleigh wave using two interdigital transducers (IDTs) to excite a bidirectional traveling wave. One IDT at a time is driven to excite the wave, and then, to drive the slider in one direction. The active IDT is changed for the alternative linear motion of the slider. For friction force, which generates the linear motion of the actuator, pressing force acting on the slider is given, so that the slider is pressing against the stator. This pressing force is called the preload.

To explain the principle of the actuator driving mechanism, a drawing in which the wave motion is enhanced is convenient to show the image. Actual wave motion is too small to present in the drawing; therefore, the displacement of wave

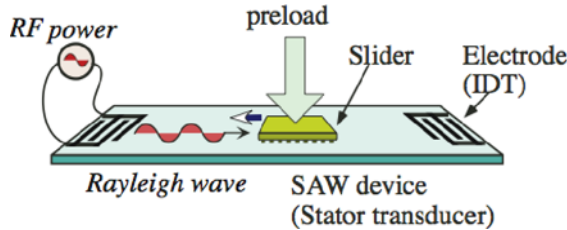


Fig. 2.1 Schematic of surface acoustic wave motor

motion is enlarged about 10,000-fold in Fig.2.2. Regarding the actual dimensions of wavelength and vibration displacements, the stator surface is almost flat; in the case of 9.6 MHz driving frequency, for example, the wavelength and vibration displacements are about 400 μm and 20 nm, respectively. Physically, therefore, the contact between the stator and the slider contains elastic deformation, stick, and slip. Under actual driving conditions, the driving frequency and the preload are maintained to be constant, and then, driving voltage is changed to control slider speed by changing wave amplitude, namely, the vibration velocity at the crests.

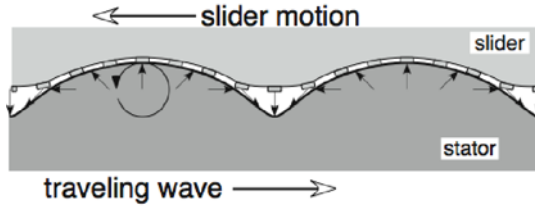


Fig. 2.2 Schematic drawing of contact between traveling wave in stator and projections on slider surface

The wave motion has two direction components; direction normal to the boundary and tangential direction. Owing to the wave motion in the stator and slider stiffness, the pressing force between the slider and the stator has distribution. Hence, around the crest of the wave, the normal force becomes large. On the contrary, at the valley of the wave, the slider surface is off. The large normal force around the wave crest is important for the frictional force in the actuator principle.

At the crest, the particles in the stator have the maximum vibration velocity in the tangential direction, which is opposite to the wave traveling direction. The large frictional force and the large tangential vibration velocity generate the linear motion of the actuator. The limit of the actuator speed is the vibration velocity of the wave crest, which depends on vibration amplitude. The limit of the actuator output force is the friction force; at the maximum, the product of the preload and the frictional coefficient between the stator and the slider.

For stable friction driving conditions, many projections are fabricated on the surface of the slider. The diameter of the projections was 20 μm or smaller to obtain a large thrust and a high speed close to vibration velocity in the case of 9.6 MHz driving frequency. It has been found from experiments that the larger the projection diameters, such as 30 or 50 μm , the lower the performance in terms of speed and thrust [4]. For the experiment, several types of silicon slider were fabricated with the dry etching process. The slider dimensions were 5x5 mm²; 2 μm high projections were fabricated in a 4x4 mm² area.

For experiments [4], the material of the SAW device was 128 degree y-rotated x-propagation LiNbO₃. The dimensions of the device were 60 mm long, 14 mm wide, and 1 mm thick. The electrodes were twenty pairs of IDTs that were 100-

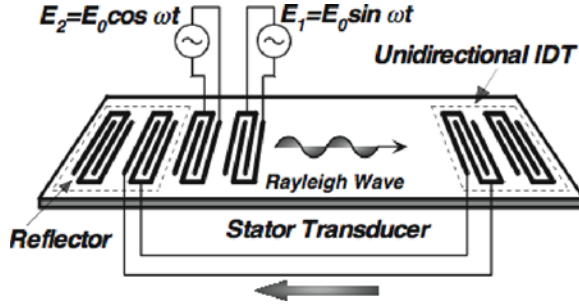


Fig. 2.3 Schematic diagram of energy circulation SAW motor

μm -wide chromium/aluminum line had a $100\ \mu\text{m}$ gap, and were $9\ \text{mm}$ in aperture. The resonance frequency, namely, the operation frequency, was $9.61\ \text{MHz}$. When the driving voltage was $125\ \text{V}_{0-p}$, the vibration amplitude and velocity were $21\ \text{nm}$ in the direction normal to the surface and $1.1\ \text{m/s}$ in tangential direction, respectively; the input power was $70\ \text{W}$.

A basic constructions of a surface acoustic wave motor is to reduce the electrical power from RF power sources two phase driving method have been proposed as shown in Fig.2.3. The principle is almost same as traveling wave excitation in circular ring/plate ultrasonic motors except for the energy conversion at the both end parts of the plate; sin and cos generators are used as drawn in Fig.2.3.

2.3 Modeling of Contact

A physical modeling of frictional drive of a SAW motor has been carried out [17-21] on the basis of contact mechanics [22]. For the first step of the modeling, a slider elastic body, a rigid projection, and a stator elastic body were expressed using four springs, one rigid body connected to the elastic slider part, and frictional boundary surfaces, as shown in Fig.2.4. In the modeling drawing shown in Fig.2.4, a_v , a_h , P , and Q are the vertical wave amplitude, the horizontal wave amplitude, the vertical direction force acting on the projection, and the thrust force acting on the projection surface, respectively. The equivalent spring constant of the slider and the stator are indicated by k_{pn} , k_{pt} , k_{sn} , and k_{st} in the normal and tangential directions, respectively.

The two springs in the sliders k_{pn} and k_{pt} can be written in the forms

$$k_{pn} = 4 G_{Si} a [\ln(3-4 \nu_{Si}) / (1-2 \nu_{Si})] \quad (2.1)$$

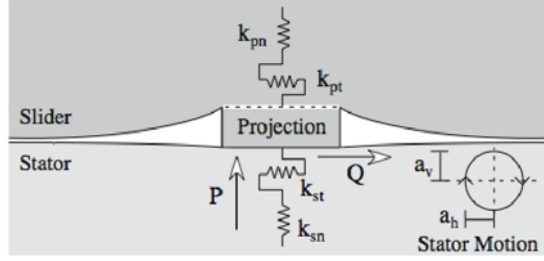


Fig. 2.4 Physical contact modeling of projection on slider and stator surface

$$k_{pt} = G_{Si} a / [1/8 + (1 - 2 \nu_{Si}) / (8 \pi \kappa)]. \quad (2.2)$$

In these equations, G_{Si} , ν_{Si} , and a are the slider material shear modulus, Poisson's ratio, and projection radius. In eq. (2.2), $\kappa = \ln(3 - 4 \nu_{Si}) / \pi$. The other two springs in the stators k_{sn} and k_{st} can be written in the forms

$$k_{sn} = 4 G_{LN} a / (1 - \nu_{LN}) \quad (2.3)$$

$$k_{st} = 8 G_{LN} a / (2 - \nu_{LN}). \quad (2.4)$$

In these equations, G_{LN} and ν_{LN} are the stator material shear modulus and the Poisson's ratio.

Using the physical model of one projection, we carried out a numerical simulation in time domain including preload, friction coefficient, vibration amplitude, and so on [23]. From the simulation, the thrust between the stator and the slider were obtained, then, the mean speed and thrust of the slider were estimated [24]. It is understood that the friction drive has two parts: sticking with elastic deformation in the nanometer range and slipping at the boundaries.

2.3.1 Estimation on Physical Model

Simulations of a SAW motor operation were carried out using the projection contact model and results were compared with experimental results at 9.6 MHz motor operation. The driving voltage was 125 V_{0-p}, so that the vibration amplitude and velocity were 21 nm in the direction normal to the surface and 1.1 m/s in tangential direction. The slider projection number was changed from 1089 to 10000 in the case of a 20-μm-diameter slider. Then, performance differences depending on the slider projection diameters ranging from 20 to 50 μm with same contact sur-

face area of about 3 mm^2 in $4 \text{ by } 4 \text{ mm}^2$ were compared with the experimental results [4, 25, 26].

The silicon material for the slider and lithium niobate for the stator are anisotropic materials. Hence, the material constants of the slider and the stator were simplified to be approximated isotropic elastic constants [13] for use in eqs. (2.1) to (2.4). The approximated isotropic elastic constants of rigidity modulus G_{Si} and Poisson's ratio ν_{Si} have been obtained using Voigt average [27], namely, $G_{\text{Si}} = 68.0 \text{ GPa}$ and $\nu_{\text{Si}} = 0.218$ [18]. For the elastic constants of lithium niobate, we then approximated to the isotropy from the propagation velocity of the Rayleigh wave and the longitudinal wave [28]; substituting those velocities to the equations of velocities of an isotropic material extracted the approximated isotropic elastic constants [28], which were $G_{\text{LN}} = 93.7 \text{ GPa}$ and $\nu_{\text{LN}} = 0.05$ [19].

It is difficult to maintain a uniform contact condition for each of the projections distributed in a $4 \times 4 \text{ mm}^2$ area, owing to the small vibration amplitude and elastic deformation in the nanometer range. Hence, the effective factor of projection contact was investigated using $20 \text{ }\mu\text{m}$ diameter, 80 projections in the line by 80 projections in the column slider. In the simulation, the number of projections was reduced by the effective factor in the line and column. For example, in the case of the effective factor of 0.6, the actual slider of 80×80 projections was reduced to 48×48 projections. In addition, in the simulation, the projection distribution in the wave traveling direction was ignored. Namely, the attenuation of the wave by the friction drive was neglected to simplify the calculation.

Using five different slides with projection numbers of 10000, 6400, 4356, 2500, and 1089, thrust and speed that were estimated by the simulation were compared with experimental results [29]; the projection diameter was $20 \text{ }\mu\text{m}$. The thrust at null speed, namely, maximum thrust, depends on the preload and the number of

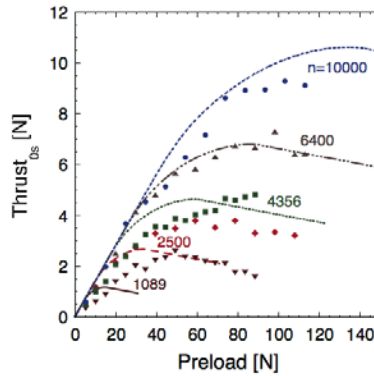


Fig. 2.5 Output force characteristics of $20\text{-}\mu\text{m}$ -diameter sliders with change in numbers of projections

the projections, as indicated in Fig.2.5. There are five curves obtained for simulation and plots for experimental results, as indicated in Fig.2.5 as follows: “ $n=10000$ ”, “6400”, and so on. From the simulation, it is understood that the stiffness at the slider contact surface is important for a large thrust. This is because the stiffness is in proportion to the number of projections. The stiff surface is suitable for high-speed operation.

A difference in slider projection diameter as a function of the output force of the SAW motor indicated interesting result, as shown in Fig.2.6 [29]. The simulation results are indicated with a dotted line, a dashed line, and a solid line for 20, 30, and 50 μm projection diameter sliders, whereas the experimental results are indicated with circles, triangles, and rectangles, respectively. Three sliders had the same contact area of 3 mm^2 but different projection diameters; the 20- μm -diameter projection slider had 10000 projections. The small diameter projections have lower stiffness than the large projections. However, the total stiffness becomes higher if the total projection contact surface area is the same as the large projection slider. It is clearly indicated in eqs. (2.1) to (2.4) that the stiffness is proportional to the radius of projections, not to the square of projection radius. Thus, if the total projection areas are the same, the smaller projection slider has a higher surface stiffness. The high surface stiffness of slider induces a large thrust. The higher surface stiffness due to small-diameter projections provides superior performance in terms of speed.

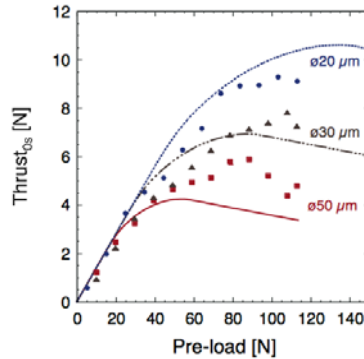


Fig. 2.6 Differences in output force characteristics between 20- μm -, 30- μm - and 50- μm -diameter projection sliders

2.4 Feedback Control

2.4.1 Experimental Setup

Material of the stator is 128 degree rotated Y-cut LiNbO_3 . The dimensions of the device were about 80 mm long, 13 mm wide and 1 mm thick. The IDTs on the stator were designed for the energy circulation drive SAW motor [15, 16]. From the dimensions of the electrode, the resonance frequency of the IDT was about 13.34 MHz.

The slider material was Si. The contacting surface was dry etched to be fabricated a lot of projections for friction drive. The contact area was 4 by 4 mm². Thin film material were used as friction material on Si slider. The materials were diamond like carbon. Thickness of the film was 0.1 μm . The slider used for the experiment had 5 μm diameter projections with intervals of 14 μm on their friction drive surface. The height of the projections was 0.5 μm .

An experimental setup is shown in Fig.2.7. On the stator device, the silicon slider is placed with applying pre-load by a plate spring. The pre-load was designed to be 8.7 N. The motion of the slider is guided with a ball bearing linear slider placed beneath the stator SAW device.

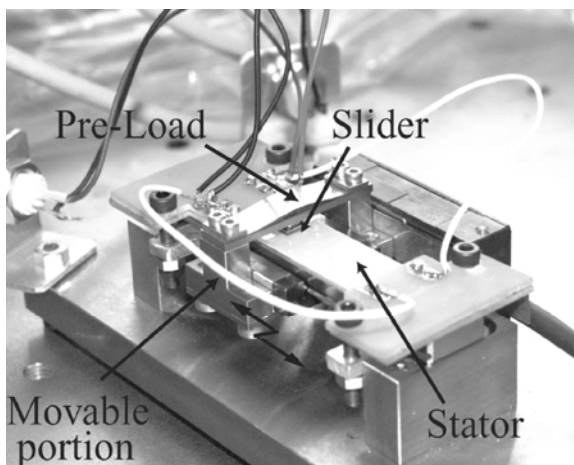


Fig. 2.7 Experimental setup

2.4.2 Response of Motor

For characterize the motor speed response, transient responses of the motor were measured by changing the driving voltage, namely, driving power. The speed of a SAW motor depends on the driving power.

Due to the unsymmetrical construction of the electrodes arrangement, the propagating power without a slider was already imbalanced. In addition, in case of forward propagation of the wave, the driving wave is directly radiated from the driving IDTs. However, in case of backward propagation, the wave generating power is once transmitted to the circulation electrodes. Hence, the losses at the unidirectional IDTs cause the power loss for the backward drive.

A problem of the SAW motor as a plant of a feed back controller is a nonlinearity. It means that the response has dead zone, for example, from $-10 V_{rms}$ to $+10 V_{rms}$. The dead zone should be considered to make a controller.

2.4.3 Controller and Response

The SAW motor was modeled by nonlinear part and a first order delay term as shown in Fig.2.8. This model is simplified for the first order approximation. Actually, acceleration at the starting points depended by the driving power, namely, driving voltage. Against the lower driving power, acceleration is smaller. Hence, the time constant indicated by 'T' in Fig.2.8 has dependence on the driving volt-

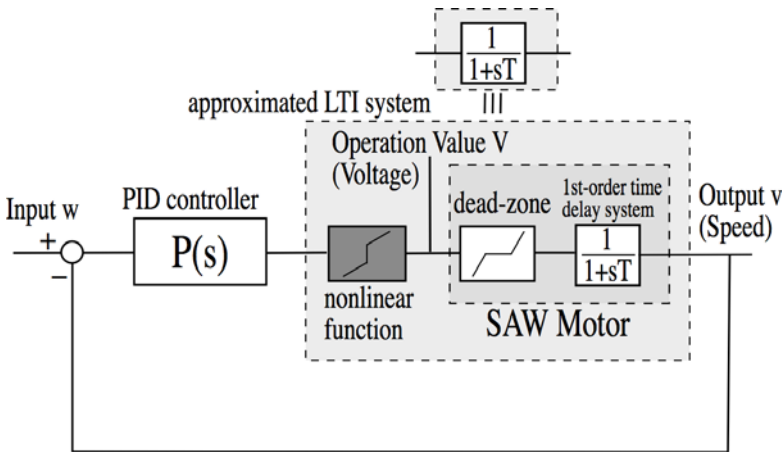


Fig. 2.8 Speed control system diagram

age. But this time, the time constant was simplified to be independent on the driving voltage.

The plant of the surface acoustic wave motor was linearized simply using nonlinear function as shown in Fig.2.8. Then, the linearized plant that has first order time delay was controlled with a simple PID feed back control system. The sinusoidal motor speed response indicated in Fig.2.9 was almost no switching distortion at around null speed.

2.4.4 Improved Modeling

The energy circulation drive SAW motor model has been improved and represented with a simple block diagram [30, 31], in case of the motor force-speed characteristic is linear. The block diagram includes the driving force function, the damping coefficient and the slider mass. By giving the driving voltage alone, the motor response in time domain, from the starting up to the stop, was obtained. The simulation model response was almost same as the actual motor response. This simple model has an advantage to build a servo control system for the SAW motor. In addition, for the versatile modeling, the block diagram will improved further.

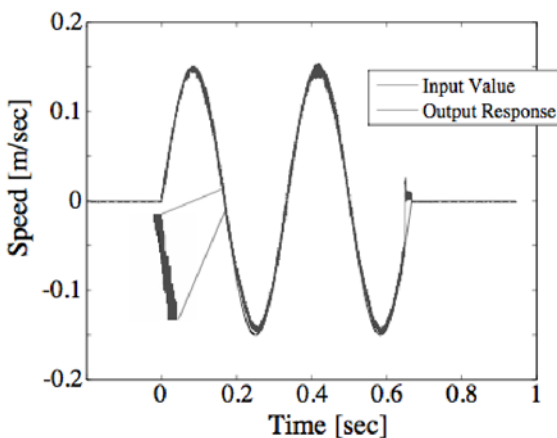


Fig. 2.9 Sinusoidal response of speed controlled SAW motor

2.5 Conclusions

It has been unclear for several years why a smaller-diameter projection slider has superior performances in terms of speed and thrust. From the physical modeling of the SAW motor based on contact mechanics, the motor operation has successfully explained about the difference in slider surface texture. The stiffness of the slider surface depends on projection diameter and the amount of projections; the smaller-diameter slider has a stiff surface if the contact areas are the same. This is because the stiffness of one projection is in proportion to the projection radius, not the square of the radius.

We demonstrated that the SAW motor response is linearized by simple nonlinear function to apply the simple PID controller for a feed back system. The motor response was improved in quick response and linearity. However, the other nonlinearity such as thrust and other factors were not considered in this work. An improved, in case of the motor force-speed characteristic is linear, simple block diagram has been proposed.

Acknowledgments This work was supported with the Ministry of Education, Science, Sports and Culture.

References

1. Kurosawa M, Takahashi M, Higuchi T (1996) Ultrasonic linear motor using surface acoustic wave. *IEEE Trans. Ultrason. Ferroelectr. Freq. Control* 43(5): 901-906
2. Kurosawa MK, Takahashi M, Higuchi T (1998) Elastic contact conditions to optimize friction drive of surface acoustic wave motor. *IEEE Trans. Ultrason. Ferroelectr. Freq. Control* 45(5): 1229-1237
3. Asai K, Kurosawa MK and Higuchi T (2000) Evaluation of the driving performance of a surface acoustic wave linear motor. *Proc. IEEE Ultrasonics Symp.*: 675-679
4. Kurosawa MK, Itoh H, Asai K, Takasaki M, Higuchi T (2001) Optimization of slider contact face geometry for surface acoustic wave motor. *Proc. of IEEE MEMS*: 252-255
5. Nakamura N, Kurosawa MK, Shigematsu T, Asai K (2003) Effects of ceramic thin film coating on friction surfaces for surface acoustic wave linear motor. *Proc. IEEE Ultrasonics Symp.*: 1766-1769
6. Shigematsu T, Kurosawa MK, Asai K (2003) Nanometer stepping drives of surface acoustic wave motor. *IEEE Trans. Ultrason. Ferroelectr. Freq. Control* 50(4): 376-385
7. Shigematsu T, Kurosawa MK, Asai K (2003) Sub-nanometer stepping drive of surface acoustic wave motor. *Proc. IEEE-NANO*: 299-302
8. Shigematsu T, Kurosawa MK (2006) *IEEJ Trans. Sens. Micromach.*, 126-E: 166
9. Iseki T, Shigematsu T, Okumura M, Sugawara T, Kurosawa MK (2006) Two-dimensionally self-holding deflection mirror using surface acoustic wave motor. *Opti. Rev.* 13: 195-200
10. Asai K, Kurosawa MK (2003) Energy circulation methods for surface acoustic wave motor. *IEICE Trans. Fundam.*, J86-A: 345-353 [in Japanese]
11. Kurosawa MK, Miyazaki Y, Shigematsu T (2007) Study of scattering by surface acoustic wave motor slider using finite element method simulation. *J. Jpn. Appl. Phys.* 46: 4915-4920
12. Asai K, Kurosawa MK (2003) Simulation model of surface acoustic wave motor considering tangential rigidity. *IEICE Trans. Fundam.*, J86-A: 1442-1452 [in Japanese]

13. Shigematsu T, Kurosawa MK (2006) Friction drive modeling of SAW motor using classical theory of contact mechanics. *Proc. Actuators*: 444-447
14. Asai K, Kurosawa MK, Higuchi T (2004) Energy circulation methods for surface acoustic wave motor. *Electronics and Communications in Japan, Part 3*, 87(2): 345-353
15. Suzuki T, Kurosawa MK, Asai K (2005) Control of a surface acoustic wave motor using PID controller. *Proceedings of LDIA*: 326-329
16. Kurosawa MK, Suzuki T, Asai K (2007) Surface acoustic wave motor using feed back controller with dead zone linearization, *J. Jpn. AEM*, 15(2): 125-131 (in Japanese)
17. Shigematsu T, Kurosawa MK (2008) Friction Drive of an SAW motor Part I: Measurements, *IEEE Trans. Ultrasonics, Ferroelectrics, and Frequency Control*, (57)9: 2005-2015
18. Shigematsu T, Kurosawa MK (2008) Friction Drive of an SAW motor Part II: Analyses, *IEEE Trans. Ultrasonics, Ferroelectrics, and Frequency Control*, (57)9: 2016-2024
19. Shigematsu T, Kurosawa MK (2008) Friction Drive of an SAW motor Part III: Modeling, *IEEE Trans. Ultrasonics, Ferroelectrics, and Frequency Control*, (57)10: 2266-2276
20. Shigematsu T, Kurosawa MK (2008) Friction Drive of an SAW motor Part IV: Physics of Contact, *IEEE Trans. Ultrasonics, Ferroelectrics, and Frequency Control*, (57)10: 2277-2287
21. Shigematsu T, Kurosawa MK (2008) Friction Drive of an SAW motor Part V: Design Criteria, *IEEE Trans. Ultrasonics, Ferroelectrics, and Frequency Control*, (57)10: 2288-2297
22. Johnson KL (1985) *Contact Mechanics*. Cambridge University Press, Cambridge, U.K.
23. Asai K, Kurosawa MK (2002) Performance estimation of surface acoustic wave motor using simulation model of friction drive. *IEICE Trans. Fundam.*, J85-A: 1428-1439 [in Japanese]
24. Mano T, Tsukimoto T, Miyake A (1992) *IEEE Trans. Ultrason. Ferroelectr. Freq. Control* 39: 668
25. Kurosawa MK, Itoh H, Asai K (2001) Influence of elastic deformation in surface acoustic wave motor friction drive. *Proc. Transducers*: 726-729
26. Kurosawa MK, Itoh H, Asai K (2003) Elastic friction drive of surface acoustic wave motor, *Ultrasonics* 41(4): 271-275
27. Hull R (ed) (1999) *Properties of Crystalline Silicon*. Inspec, London
28. Kushibiki J, Takanaga I, Arakawa M, Sannomiya T (1999) *IEEE Trans. Ultrason. Ferroelectr. Freq. Control* 46: 1315
29. Kurosawa MK, Shigematsu T (2008) Friction drive simulation of surface acoustic wave motor characteristics based on contact mechanics, *Jpn. J. Appl. Phys.*, 47(5): 4287-4291
30. Okano M, Kurosawa MK (2007) Study on modeling of surface acoustic wave motor. *Proc. of IEEE Int. Symp. on Industrial Electronics*: 1508-1513
31. Okano M, Kurosawa MK (2008) Model based position control of surface acoustic wave motor. *Proc. of Actuator*: 172-175

Next-Generation Actuators Leading Breakthroughs

Higuchi, T.; Suzumori, K.; Tadokoro, S. (Eds.)

2010, XXII, 438 p., Hardcover

ISBN: 978-1-84882-990-9